Experimental investigation and modelling of the interaction between an AVR and ballast load frequency controller in a stand alone micro-hydroelectric system

R. Jarman, P. Bryce

Faculty of Engineering University of Technology, Sydney

Broadway NSW 2007 Australia

Abstract

Extensive field experience in micro-hydroelectric systems in remote rural communities demonstrates that the use of a typical Automatic Voltage Regulator (AVR), as supplied with a brushless self exciting synchronous alternator, can be the cause of unsatisfactory system performance. This paper presents results from experiments undertaken on a full scale micro-hydroelectric test rig as well as system modelling with PSCAD. The source of the instability is considered to stem from the similar time constants of the ballast load frequency controller and the AVR as two competing feedback control systems. System modelling is used to verify steady state operating points, and confirms that the under frequency roll-off (UFRO) characteristic of the AVR also contributes to unsatisfactory performance.

Keywords: micro-hydroelectric, frequency control, remote power supplies, renewable energy

---

1. Introduction

Extensive field experience in stand alone micro-hydroelectric systems in developing communities in the South Pacific [1, 2, 3] demonstrates the use of a typical Automatic Voltage Regulator (AVR) as supplied with a brushless self exciting synchronous alternator can be the cause of unsatisfactory system performance. In these systems, a binary weighted ballast load frequency controller is used to govern alternator speed, and hence regulate system frequency.

This paper reviews literature describing similar observations, and reports on the results obtained from experiments conducted on a full scale micro-hydroelectric test rig. System modelling and simulation with PSCAD verifies the proposition that the cause is related to the similar time constants of the two feedback systems. This work also reveals that the Under Frequency Roll-Off (UFRO) characteristic of the automatic voltage regulation (AVR) plays a role in unsatisfactory system performance.

2. Ballast load frequency controlled micro-hydroelectric system

In a typical APACE VFEG* micro-hydroelectric system (generating capacity < 100 kW), electricity is generated at 240 V_{AC} 50 Hz via a standard off-the-shelf brushless self excited synchronous alternator. These run-of-the-river schemes convert the kinetic energy of falling water to rotational energy, typically via a pelton wheel or cross flow water turbine. The rotational velocity of the alternator shaft (ω_m) and hence frequency (f) is regulated by balancing the system torque equation at a nominal set-point speed – typically 1500 RPM for a 4 pole alternator.

$$T_{shaft} - T_{load} = T_{acceleration} = J \frac{d\omega_m}{dt} \qquad \text{[Nm]} \qquad (1)$$

The turbine supplies the shaft torque to the alternator. The opposing load torque is made up of the alternator electromagnetic torque and system losses. The system moment of inertia (J) for a pelton turbine, alternator rotor and associated pulley systems is in the order of 0.55 kgm^2 for a typical 40 kW system.

A ballast load frequency controller switches resistive load (ballast) to increase or decrease electromagnetic torque produced by the alternator, regulating shaft speed, and hence system frequency. Variations in system frequency as a result of changes in consumer demand as well as long term seasonal variations in water supply are accounted for in the controller algorithm. The specific controller in our field work is based on an 8 bit microcontroller; input signals include measured system frequency, outputs include (up to) eight digital outputs which control solid state relays switching the resistive load elements. Presently, the AVR supplied by the alternator manufacturer is replaced with a fixed (but user adjustable) exciter field current derived from a linear power supply circuit, based on a typical transformer, bridge rectifier and linear regulator circuit. System voltage is then proportional to frequency, and regulated by the frequency controller. A limitation of this fixed field current solution is its inability to automatically adjust for variations in system power factor; local community users' policy/governance mitigates this to an extent by restricting consumers to near unity power factor loads. Another limitation of the fixed field supply is its inability to automatically adjust for (usually seasonal) variations in input water power and hence appropriate exciter current for the alternator load. This task must be completed manually by village technicians and adds to training and risk management demands.

3. Summary of literature

Excitation requirements for synchronous machines in these systems is not as simple as first thought [4]. Published [5] and observed evidence suggests it is nearly impossible to get an AVR excited machine to steady state in this stand-alone turbine-driven application. The practical implications of bringing the alternator up to running speed described by the AVR manufacturer [6] confirm the same – in a diesel generator system, the separate speed governor is used to set and regulate engine speed. In these micro-hydro systems, the speed is regulated by balancing alternator shaft torques, not by controlling turbine water power input.

Moreover, AVR's are a common failure in micro-hydroelectric systems, and engineers are advised to keep stocks of spare AVR's and diodes [7]. Designers and practitioners have proposed a variety of reasons and responses to these oft-experienced component failures and functional inadequacies. The reasons for poor reliability are thought to stem from the use of thyristor type load controllers imposing electrical and mechanical loading on the AVR which will shorten its life. In addition low speed running

of the turbine and generator may occur for prolonged periods, unlike the conditions anticipated in the diesel engine – generator combination for which AVR's were designed. In such conditions the AVR may respond by boosting the excitation in order to raise output voltage, but will be unable to do this continuously without overheating. A solution proposed is to purchase an AVR with a more robust specification [7, 8].

Thirdly, unstable operation during consumer load changes have been predicted [9], the interaction between load controller and AVR has been considered the source of instability [10], and one suggestion included 'dumbing down' the frequency controller [9]. The suggestion has also been made that two stable operating points may exist for the one turbine opening, as an explanation for an observed 45-55 Hz instability (or hunting) [5]. Predictions of a minimum system moment of inertia requirement for stable operation (around 3.2 kgm^2 for a 40 kW system) have been made [11, 12]. Some designers [13, 14, 15] added flywheels to the alternator shafts to overcome instability, and then went on to develop various rationale to explain why or how it works. As a comparison, the moment of inertia for a typical 40 kW diesel engine driven system is around 4.5 kgm^2 [16].

The experimental and modelling results discussed below provide dome clarity on these surmised difficulties surrounding the use of commercial AVR's, and offer a way forward for expanding applications to low inertia machines.

4. Experimental verification of instability

The Renewable Energy Laboratory in the Faculty of Engineering at the University of Technology, Sydney houses a full scale micro-hydroelectric system. This system and its associated data acquisition components have been used in the research and development of numerous specialized components for micro hydroelectric systems. Figure 1 shows a sketch of the main system components.

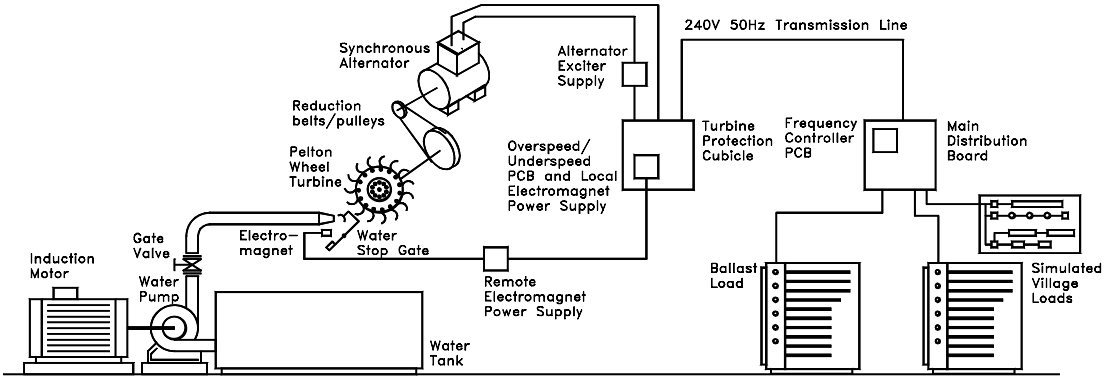

Figure 1. Main system components of the UTS micro-hydroelectric test rig in the Renewable Energy Laboratory

A set of experiments were conducted to measure and record various parameters as the system became unstable. The micro-hydro system was set up exactly as it would be in the field. Figure 2 compares the graphs for an increase and then decrease in water power; the graphs on the left hand side show the system with fixed excitation and ballast load controller, on the right show the system with the fixed excitation replaced by a the manufacturer's standard (commercial) AVR controlled excitation and ballast load controller.

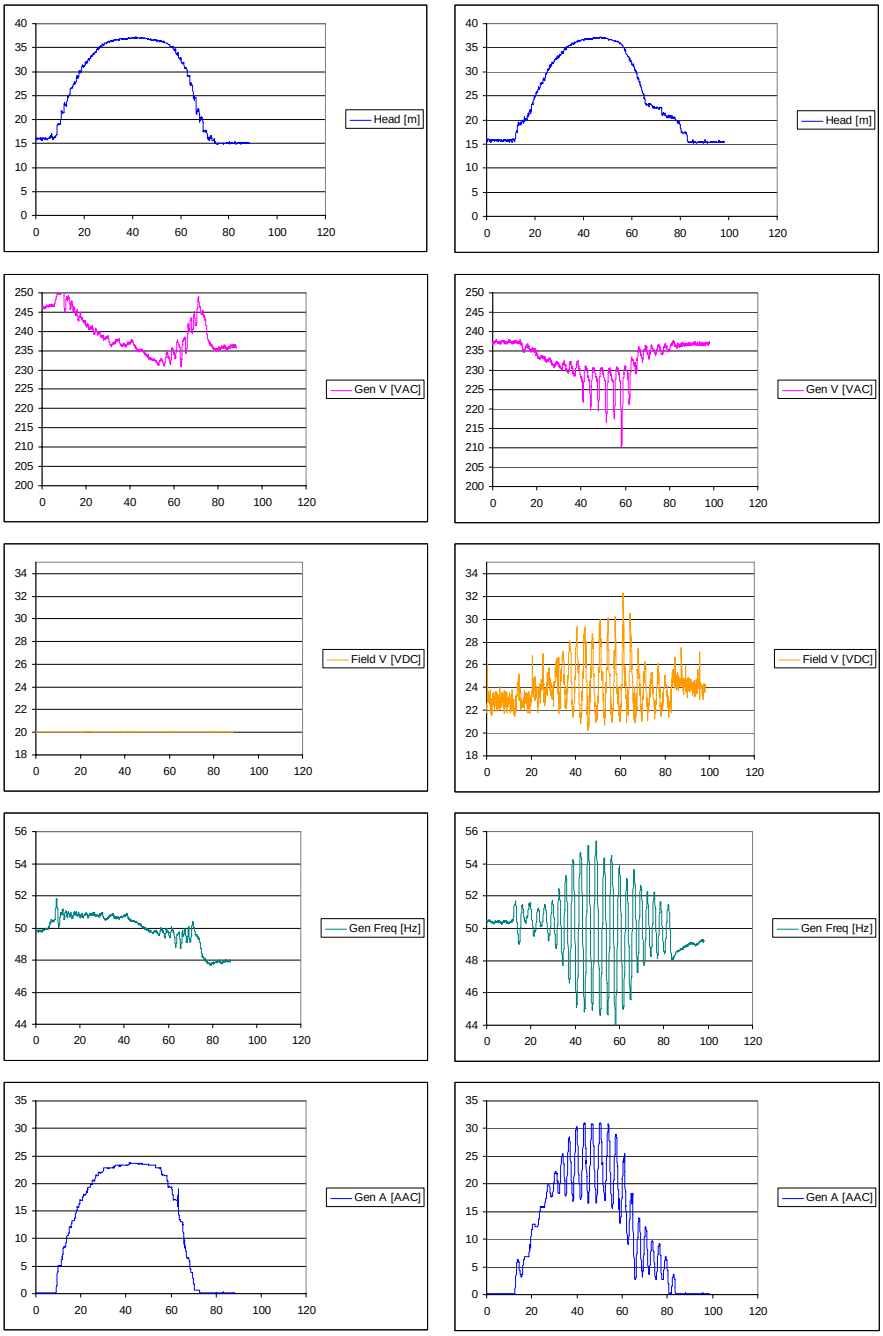

Figure 2. Graphs comparing the response of various system parameters versus time [sec] for an increase and decrease in hydro power with the ballast load frequency controller and linear regulator exciter supply (left hand side), and AVR controlled exciter supply (right hand side).

A gate valve was used to vary water power input to the turbine. Measurements from flow and head sensors indicated a near linear relationship between water head and flow over the range of interest in these experiments. A water head input of around 15 metres (and flow = 12 litres/sec) established a steady state operating point where the system losses and electrical excitation balanced the water power input.

This point represents the starting point, shown on the left hand side of the graphs. The graphs show the variation of water power into the turbine as varied over approximately 80 seconds, and are slightly different since this operation was performed manually.

Significant points of interest for the fixed excitation graphs include:

(a) the shape of the alternator current is the same as the water head since system voltage remains near constant, and electrical power balances water power input,

(b) the ballast load frequency controller maintains system frequency at about 50 Hz,

(c) terminal voltage drops with increased load on the alternator.

Significant points for the AVR controlled excitation graphs include:

(d) the AVR increases field current with increased load on the alternator,

(e) oscillations in system frequency develop and increase as soon as water input increased,

(f) at the point where the oscillations in system frequency are a maximum, each transit below 45 Hz results in an immediate reduction in terminal voltage,

(g) the oscillations could only be stopped by reducing the water power input to the turbine.

Oscillations in the system frequency and alternator current were apparent from an early stage in the experiment. The causes are thought to stem from the similar time constants of the ballast load frequency controller and the AVR. Additionally, the transients described in point of interest (f) can be seen to contribute, although they are not responsible for the initial development of the unstable oscillations. The causes of these latter transients stem from the under-frequency-roll-off (UFRO) characteristic of an AVR, and are further discussed below.

Not apparent in the experimental results for the AVR excited system is the difficulty in obtaining the initial steady state operating point. This state must be achieved without the use of the frequency controller and requires careful manual adjustment of water input and resistive load, usually taking a number of attempts to accomplish. This is the practical implication described in the summary of literature above and is independent of lab or village context. However, the results shown here represent a conceptual starting point – that is, assume the system is in steady state and then observe what happens when a change is made. Regardless of this, the key outcome is an experimental verification of the instability, with the benefit of instrumentation not generally available when the phenomenon is experienced in the field. System modelling should assist in verifying its causes.

5. System modelling

Modelling of the hydraulic system components yields the expected parabolic shape of the power versus speed curve [17] for any given water input. Figure 3 graphs the measured electrical power versus speed characteristic for a water head input of 16.4 metres (water head is used as a convenient measurand of input water power since it is the gate valve which is adjusted). Most of the measured data points lie on the second order line of best fit; these are system steady state operating points. The data was obtained by manually switching a six-element binary weighted load resistance in 64 discrete steps. Notable are four of the intermediate transients from larger step changes in this process, and further discussion of these is presented below.

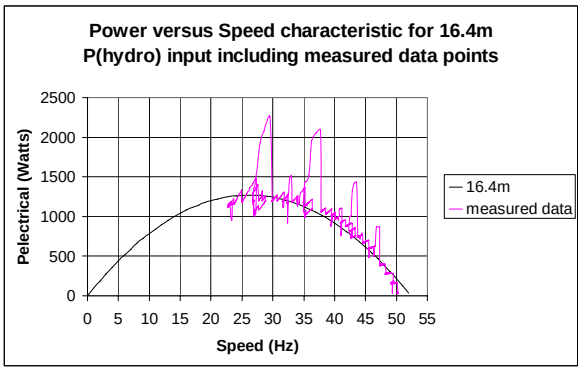

Figure 3. Experimental determination of the turbine power versus speed curve. A second order line of best fit was used to characterize the parabolic shape of the curve.

Repeating the experiment with a range of water power input yields a set of (ideal) parabolic curves. These curves give rise to the turbine speed-versus–torque family of characteristic shown in Figure 4.

Importantly, only a limited range [$125 < \omega_m < 189$ rad/sec] of these curves is considered representative for modelling purposes. Each straight line represents a specific water power input characterised by corresponding water head in meters.

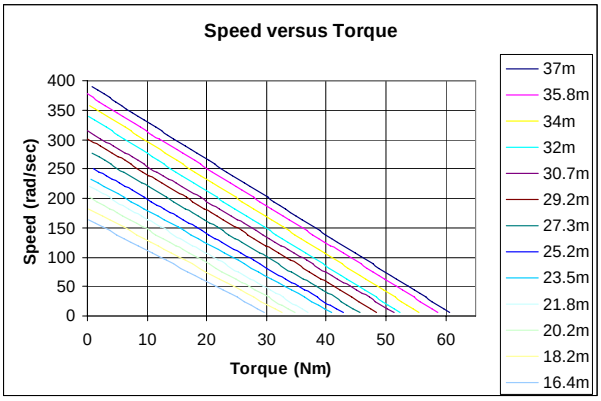

Figure 4. Turbine speed (angular velocity) versus load torque [Nm] for various water head [m] input

System equations include equation for rotational speed (ω_m)of the turbine:

$$\omega_m(s) = T_{LOAD}\frac{K_1}{1+sT_1} \quad \text{[rad/sec]} \tag{2}$$

where T_{LOAD} is the load torque applied to the shaft (sum of electromagnetic and losses), K_1 is a function of the speed-torque curves shown in figure 4, and T_1 is proportional to the laboratory system total moment of inertia J = 0.35 kgm^2.

Modelling of the electrical system components yields an equivalent first order representation of the alternator shown in Figure 5. The exciter field winding is represented as a series RL circuit between the exciter field terminals F+ and F-. The alternator in the laboratory, typical of those in the field, is a Newage International BCI-184 which has stator windings configured zig-zag single phase, and has an equivalent rating of 18.1 kVA. The maximum output from the lab system is significantly less, around 7 kW, constrained by water pump and turbine characteristics.

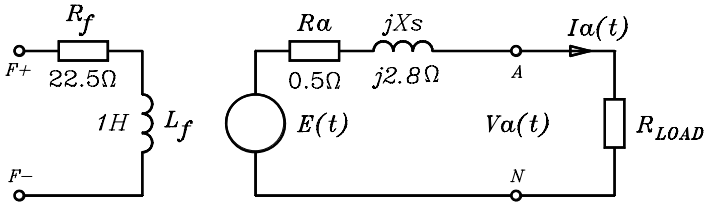

Figure 5. Electrical circuit representation of the (equivalent) single phase brushless self excited synchronous alternator

The magnitude of the alternator induced voltage (E) derived from Faraday's Law [18]:

$$|E| = 4.44N\phi f \quad \text{[V]} \tag{3}$$

where N is the number of turns in the stator winding, ϕ is the air gap flux, and f is the electrical system frequency in Hz.

The equation for electrical power generated by the alternator [18]:

$$P_e = \frac{|E||V_a|}{X_S} \sin \delta \quad \text{[W]} \tag{4}$$

where V_a is the alternator terminal voltage, δ is the alternator load angle (the phase angle between the reference alternator terminal voltage V_a and the alternator induced voltage (E), and X_S is the equivalent alternator synchronous reactance. For the unity power factor system shown in figure 5, the load angle is:

$$\delta^\circ = \tan^{-1}\left[\frac{X_S}{R_{LOAD} + R_a}\right] \quad \text{[deg]} \tag{5}$$

PSCAD, a graphical user interface for use with power systems simulations programs, was used to model the hydraulic and electrical systems. PSCAD also enabled simulations with DC and AVR controlled excitation, with and without the ballast load frequency controller. Figure 6 shows a comparison of the measured open loop (no frequency controller) system step-response with those modelled in the PSCAD simulation environment. The step response experiment consisted of bringing the system up to a steady state operating speed, generating around 2 kW. At t = 5 sec, a 1 kW step load is applied, and then rejected at t = 20 sec.

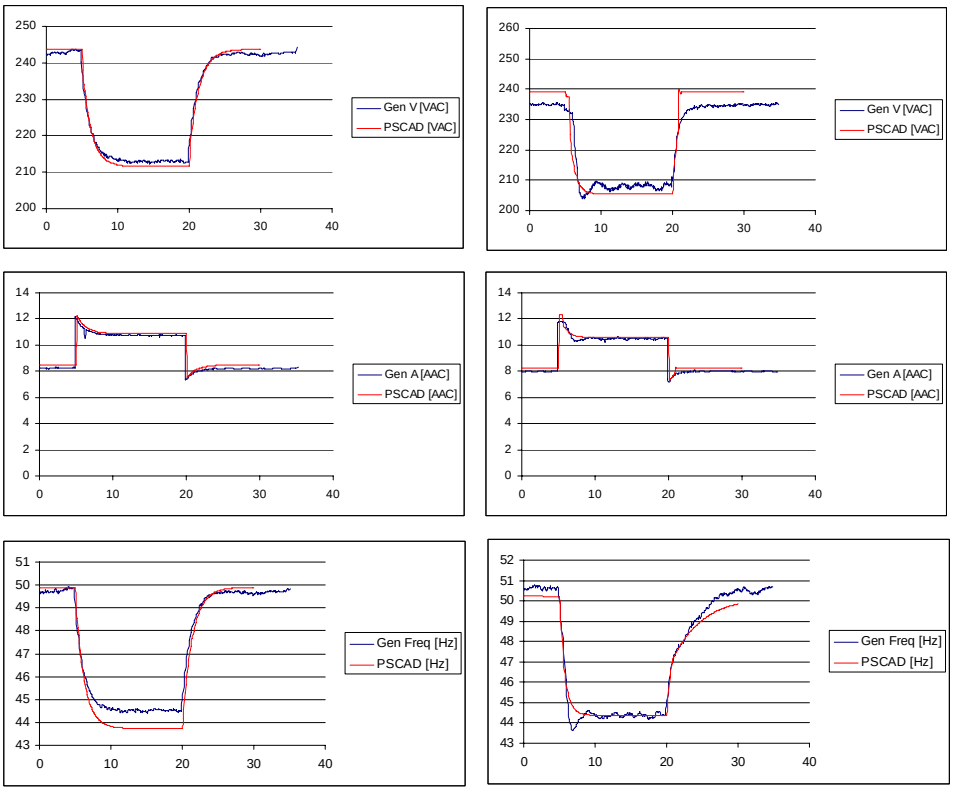

Figure 6. Comparisons of measured versus simulated step response versus time (sec) for open loop system. Graphs on the left hand side are for constant DC excited system, graphs on the right hand side are for AVR excited system. Graphs include terminal voltage (Gen V) [V_{AC}], alternator current (Gen A) [A_{AC}] and system frequency (Gen Freq) [Hz].

Overall, the simulation results represent a close comparison to the measured system variables. These open loop results formed the bases for additional work which compared the observed and predicted results of including the ballast frequency controller (closed loop step response).

Figure 7 shows a comparison of the measured closed loop (with frequency controller) system step-response with those modelled in the PSCAD simulation environment. As above, the step response experiment consisted of bringing the system up to a steady state operating speed, generating around 2 kW. At t = 5 sec, a 1 kW step load is applied, and then rejected at t = 20sec.

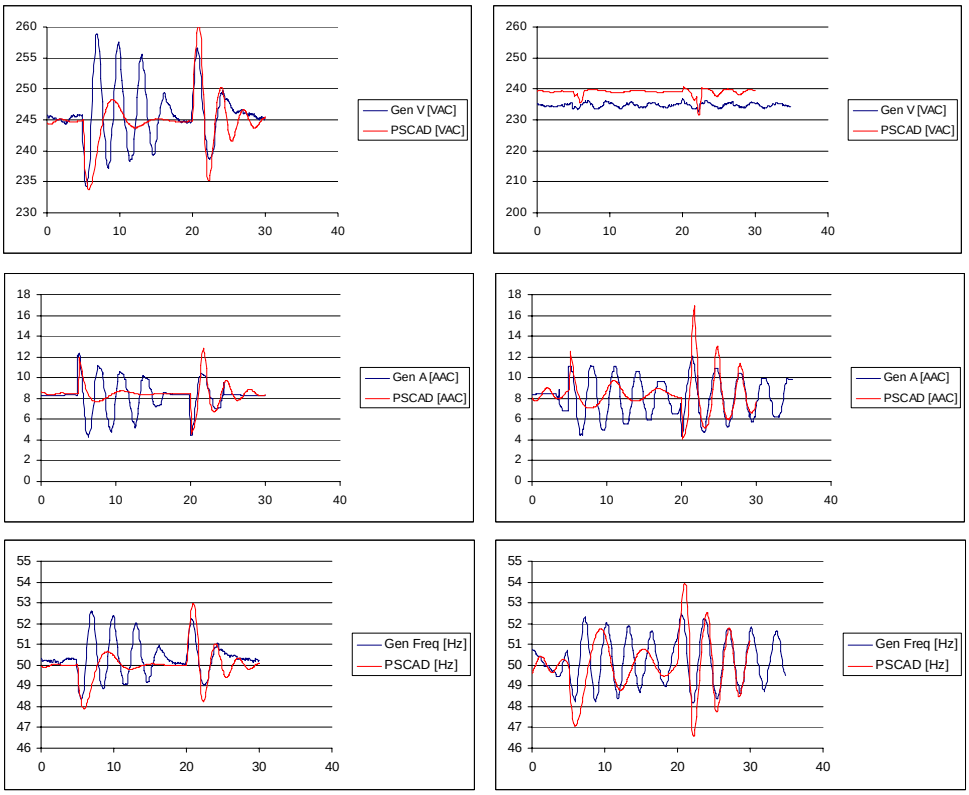

Figure 7. Comparisons of measured versus simulated step response versus time (sec) for closed loop system. Graphs on the left hand side are for constant DC excited system, graphs on the right hand side are for AVR excited system. Graphs include terminal voltage (Gen V) [V_{AC}], alternator current (Gen A) [A_{AC}] and system frequency (Gen Freq) [Hz].

Some observations of the graphs in Figure 7: Firstly, it should be noted the 1 kW_e load change represents a 50% step change in generated capacity, a much more severe step change than would normally be experienced in the field. A more typical (say < 10% step change) results in ±2% change in system voltage and frequency. Furthermore, the ballast load controller was not optimally tuned for these tests, but was representative of a typical system installation.

Secondly, the PSCAD model for the ballast load controller is based on a typical PID control strategy which has continuous and infinitely variable output control. The algorithm in the real ballast load controller is more complex, includes dead-bands and wait delays, is constrained to just 64 discrete output states, and these states are switched at zero crossings of the alternator voltage by solid state relays to reduce harmonics.

Thirdly, the system with constant DC excitation recovers to the initial steady state within approximately 10 sec. The graphs for the AVR controlled excitation system suggest a significantly longer recovery time

– approaching 60 seconds. Further, the percent excursion or overshoot from the 50 Hz set-point is much greater for the AVR controlled system compared to the constant DC excitation system.

Finally, it is apparent the step response for the AVR controlled excitation system shows a trend towards a steady state – albeit slowly as noted above. Modelling and experiments have revealed that for low water head (water power) input, a system with AVR controlled excitation can operate satisfactorily on the right hand side of the turbine power versus speed curves (described below). However, the manual adjustment required to maintain the system in this carefully balanced state makes it untenable. Further, in the experiment described in section 4, the system instability is most evident when the hydro power input (water head) is at a maximum (> 35m) which corresponds to operating on the left hand side of the turbine power speed curve.

6. Possible causes of the instability

This paper will continue to focus on understanding the cause of the unstable oscillations.

6.1 Similar time constants of control system components

The cause is considered to be related to the similar time constants of the two control system components – the ballast load frequency controller and the AVR. Analysis of the operation of the ballast load frequency controller indicates it has a time constant of around 60ms. IEEE 421.5-1992 suggests a type AC5A [19] AVR model appropriate for this sized machine has a time constant of around 20 ms. Figure 6 shows the moment of inertia of the system results in a time constant of around 1 sec. The time constant for the alternator (armature winding) electrical components is orders of magnitude faster (typically less than 1ms), and approaches zero for the purpose of this analysis.

Kirchhoff's Laws yield the equivalent electrical circuital expression for figure 5:

$$E\angle\delta = \hat{I}_a(R_a + jX_S) + \hat{I}_a R_{LOAD} \quad \text{[V]} \tag{6}$$

where I_a is the alternator current, R_a and jX_S are the armature resistance and reactance, $R_{LOAD} = (R_{BALLAST}{}^{-1} + R_{VILLAGE}{}^{-1})^{-1}$ and $R_{VILLAGE}$ represents the equivalent resistance of the consumer load, $R_{BALLAST}$ represents the equivalent resistance of the resistance switched by the ballast load frequency controller. Alternator terminal voltage $V_a\angle 0^\circ = \hat{I}_a R_{LOAD}$ is typically designated as the reference angle in the system; armature current is in phase in this unity power system.

Equations (3) and (6) model the alternator induced voltage (*E*), and will be used to describe the interaction between the various control systems.

6.1.1. Case 1: Hydro turbine with constant DC excitation and no ballast load frequency controller.

This scenario results in the graphs shown on the left hand side of figure 6. The steady state operation at *t* = 0 is described by equation (1):

$$T_{shaft} = T_{load} = T_{acceleration} = 0 \quad [\text{Nm}] \tag{7}$$

Equation (3) is rewritten:

$$|E| = 4.44\, fN\phi = k_1 f \quad [\text{V}] \tag{8}$$

where $k_1 = 4.44N\phi$ and remains constant, and frequency (*f*) can vary.

Equation (6) can be described:

$$E\angle\delta = \hat{I}_a[\underbrace{R_a + jX_S}_{unchanged} + (R_{VILLAGE}{}^{-1} + \underbrace{R_{BALLAST}{}^{-1}}_{unchanged})^{-1}] \quad [\text{V}] \tag{9}$$

where it is assumed (R_a+jX_S) remains unchanged, and $R_{BALLAST}$ remains unchanged since there is no ballast load controller.

At *t* = 5 sec, a change (*stimulus*) in village load resulted in a new $R'_{VILLAGE} = R_{VILLAGE} + \Delta R_{VILLAGE}$ causing in a near instantaneous ($\tau \to 0$) change in alternator current and machine load angle:

$$E\angle \underset{\tau\to 0}{\delta'} = \underset{\tau\to 0}{\hat{I}_a'}[\underbrace{R_a + jX_S}_{unchanged} + (\underbrace{R'_{VILLAGE}{}^{-1}}_{stimulus} + \underbrace{R_{BALLAST}{}^{-1}}_{unchanged})^{-1}] \quad [\text{V}] \tag{10}$$

where $\hat{I}_a' = \hat{I}_a + \Delta\hat{I}_a$ and $\delta' = \delta + \Delta\delta$. The time constants for these changes are determined by electrical system components, typically in the order of milliseconds, and compared to the rotating system time constants are considered negligible. The magnitude of induced voltage remains unchanged at this point since frequency has not changed.

Furthermore, the change in armature current results in a change in electromagnetic torque. Equation (1) yields a net accelerating torque which (in time) altered system speed (ω_m) according to figure 4 at a rate defined by the moment of inertia (*J*) in equation (2). Figure 6 indicates a time constant of around ($\tau \approx 1000$ ms).

The final steady state operating point is:

$$E'\angle\delta'' = \hat{I}_a''[\underbrace{R_a + jX_S}_{unchanged} + (\underbrace{R'_{VILLAGE}{}^{-1}}_{stimulus} + \underbrace{R_{BALLAST}{}^{-1}}_{unchanged})^{-1}] \quad [\text{V}] \tag{11}$$

where a new steady state induced voltage and load angle $E' \angle \delta$" results in a new steady state armature current I_a".

In summary, for the case of a hydro turbine with constant DC excitation and no ballast load frequency controller, a change (or stimulus) in $R_{VILLAGE}$ results in a change in induced voltage as a function of system speed (ω_m) as described by:

$$\underset{f(\Delta\omega_m)}{\Delta|E|} = k_1 \underset{\tau \approx 1000ms}{\Delta f} \quad [\text{V}] \tag{12}$$

6.1.2. Case 2: Hydro turbine with constant DC excitation and with ballast load frequency controller.

This scenario results in the graphs shown on the left hand side of figure 7. Following a similar analysis to that described above yields equations (7) to (10) as applicable. However, the change in system speed (ω_m) brought about by net accelerating torque resulted in ballast load controller action (τ≈60 ms). Hence, over the transient period from t = 5 sec to t = 20 sec:

$$\underset{f(\omega_m)}{E} \angle \underset{\tau \to 0}{\delta'} = \underset{\tau \to 0}{\hat{I}_a'} [\underbrace{R_a + jX_S}_{unchanged} + \underbrace{(R'_{VILLAGE}}_{stimulus}{}^{-1} + R'_{\underset{\tau \approx 60ms}{BALLAST}}{}^{-1})^{-1}] \quad [\text{V}] \tag{13}$$

where $R'_{BALLAST} = R_{BALLAST} + \Delta R_{BALLAST}$. The transient period ends when the controller returns the systems to the initial steady state operating point. Importantly, changes in induced voltage remain a function of system speed only as described by equation (12).

6.1.3. Case 3: Hydro turbine with AVR controlled excitation and no ballast load frequency controller.

This scenario results in the graphs shown on the right hand side of figure 6. Equation (3) is rewritten:

$$|E| = 4.44 fN\phi = k_2 f\phi \quad [\text{V}] \tag{14}$$

where $k_2 = 4.44N$ and remains constant, and frequency (f) and air gap flux (ϕ) can vary. Air gap flux is changed by the AVR as it varies exciter field current to maintain (regulate) alternator terminal voltage. Equations (9) and (10) hold true in this case as well. However, the change in alternator terminal voltage $V_a \angle 0° = \hat{I}_a R_{LOAD}$ resulted in AVR control action. The rate of change of terminal voltage and system frequency is noticeably greater for the AVR controlled excitation compared to constant excitation as the AVR increases field current in an attempt to maintain terminal voltage regulation. Once the system frequency fell below the UFRO set-point, the field current was reduced, and a small overshoot in the

measured response is noticeable as the system reaches a new steady state operating point. This new steady state point is similar to, but different from, the point described by equation (11).

In summary, the induced voltage (E) is a function of air gap flux (which is constrained by the UFRO characteristic) as well as changes in system frequency:

$$\underset{f(\varpi_m,\phi_{UFRO})}{\Delta|E|} = k_2 f \underset{\tau\approx 20ms}{\Delta\phi} + k_2\phi \underset{\tau\approx 1000ms}{\Delta f} \quad [\mathrm{V}] \tag{15}$$

6.1.4. Case 4: Hydro turbine with AVR controlled excitation and with ballast load frequency controller.

This scenario results in the graphs shown on the right hand side of figure 7. Equation (13) is applicable, but as described in sections 6.1.2 and 6.1.3, the stimulus will result in AVR as well as ballast load controller action, hence equation (14) becomes:

$$\underset{f(\Delta\varpi_m,\Delta\phi)}{\Delta|E|} = k_2 f \underset{\tau\approx 20ms}{\Delta\phi} + k_2\phi \underset{\tau\approx 60ms}{\Delta f} \quad [\mathrm{V}] \tag{16}$$

The significant underdamped response from the similar magnitude of the time constants for the two independent feedback control systems acting upon the one system variable.

6.1.5. Case 5: Hydro turbine with AVR controlled excitation and with ballast load frequency controller and increased system moment of inertia (eg. flywheel added to shaft of alternator).

By increasing the system moment of inertia and hence slowing the rate of change of system speed [15] the impact of the two control systems time constants are separated. The time constants associated with the system moment of inertia dominate and system behaves in a similar manner to a governed prime mover such as a diesel engine (eg. J = 4.55 kgm^2), and hence $\tau\approx$13000ms for changes in system speed and frequency. Equation (15) becomes:

$$\underset{f(\Delta\varpi_m,\Delta\phi)}{\Delta|E|} = k_2 f \underset{\tau\approx 20ms}{\Delta\phi} + k_2\phi \underset{\tau\approx 13000ms}{\Delta f} \quad [\mathrm{V}] \tag{16}$$

This system is characterised by relatively tight voltage regulation but poorer frequency regulation [14].

6.2 Impact of the AVR under frequency roll off (UFRO) characteristic

In diesel genset applications, when a large load is applied to the alternator resulting in significant speed reduction, the UFRO characteristic is useful in reducing system excitation, and hence terminal voltage

and electromagnetic torque. This affords the independent diesel engine governing system an opportunity to recover nominal speed.

When the UFRO function is applied to the different dynamic of a small turbine as prime mover, the effects become problematic. The point of interest (f), described in Section 4 above, is shown in closer detail in Figure 8. The amount by which the terminal voltage is reduced for each excursion below the UFRO set point is predicted by the AVR manufacturer, as reproduced in figure 9.

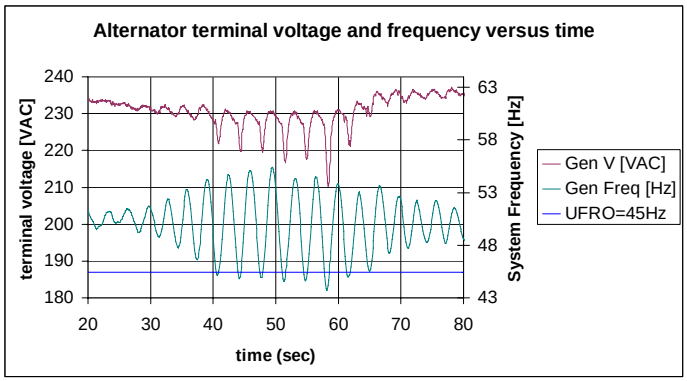

Figure 8. Graph comparing alternator terminal voltage [V_{AC}] and system frequency [Hz] showing the impact of the AVR's UFRO characteristic. Each excursion below the 45 Hz setpoint results in a decrease in AVR output, hence dropping the alternator voltage.

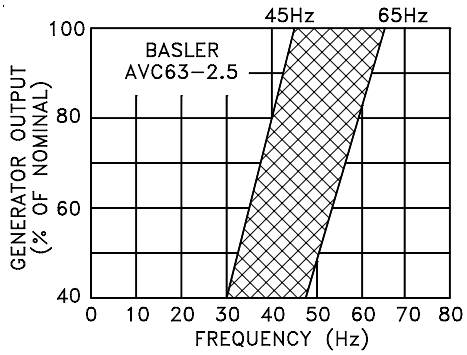

Figure 9. Graph of the Under Frequency Roll-off characteristic for the Basler AVC63-2.5 AVR [20]

This feature is user settable, the shaded region in Figure 9 shows the region of operation for an AVR resulting in reduced output from the alternator as a function of frequency. This characteristic is typical across a range of AVR manufacturers. In this case, the UFRO was set at 45 Hz, and so the largest excursion below 45 Hz in figure 7 (at around 58 seconds, when the frequency reached 43.5 Hz) the output voltage was reduced to approx 88% of 240 V_{AC}, or around 210 V_{AC} as shown in figure 8.

As noted previously, although the impact of the UFRO characteristic is not the initial cause of the instability observed in figure 2, it is clear it does contribute to unsatisfactory system performance. Apart

from these transient instabilities, the UFRO characteristic also contributes to problems in maintaining a satisfactory steady state point [5]. To understand these problems, knowledge of the system steady state operating points is required.

7. Operating points on the turbine power versus speed curves

Repeating the experiments that produced the graphs in figure 3 for a range of water power input (a function of water head in this paper) yields a family of parabolic shaped curves of the turbine power versus speed characteristic. Assuming the alternator has constant excitation, a family of parabolic resistive load power curves can mapped onto the turbine power graph as shown in figure 10.

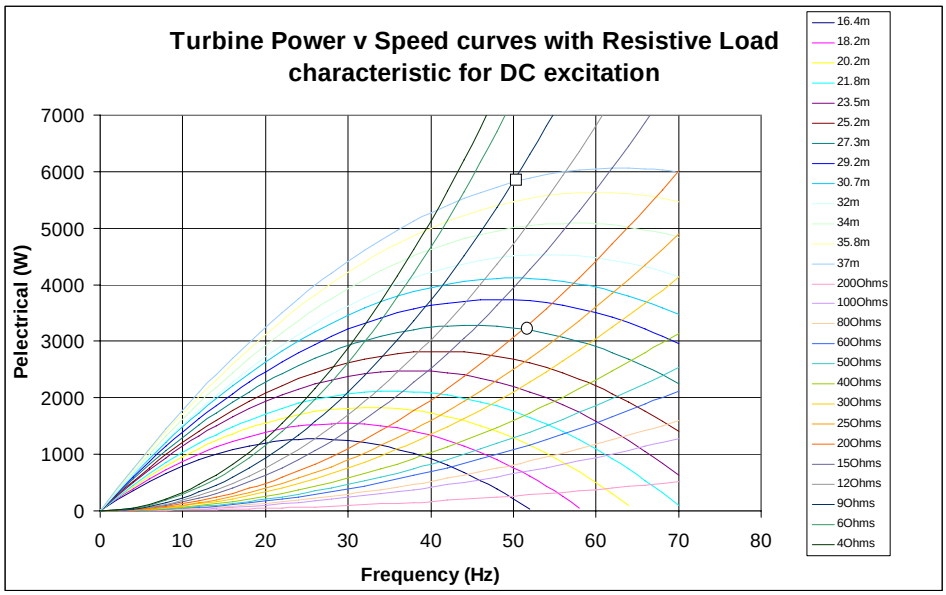

Figure 10. Steady state electrical power versus frequency for various water head input, with various Resistive Load characteristic curves for constant DC excitation.

The intersection of a turbine power versus speed curve and resistive load curve represents a steady state operating point. For example, if the water input (head) was set at 27.3 m, and the ballast load was set at 20 Ω, then the system would reach a stead state operating speed (frequency) of around 52 Hz and P_{elect} approximately 3.2 kW. This point is indicated with an **O** in figure 10. Similarly, a water input of 37 m with resistive load of 9 Ω would result in a frequency of 50 Hz and P_{elect} approximately 5.8 kW (marked with an **€** in figure 10).

A trajectory of measured data from step response experiments can be plotted onto these curves. Figure 11 shows a reduced set of curves to those shown in figure 10 for clarity. A steady state operating point exists at (50 Hz, 2 kW) representing the intersection of head = 22 m and resistive load = 28 Ω.

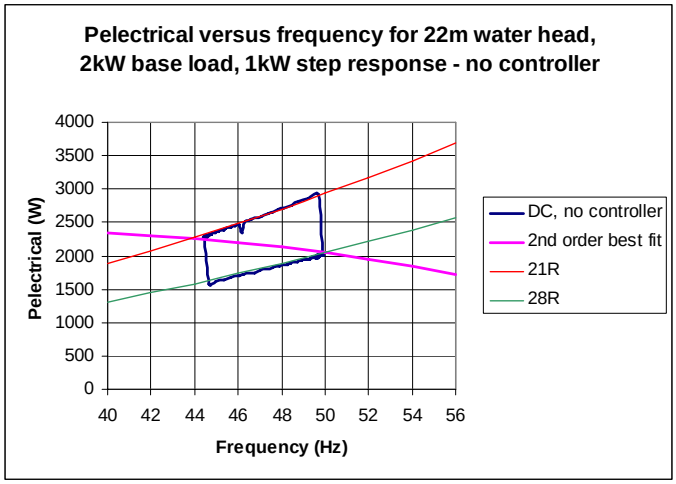

Figure 11. Trajectory for P_{elect} during load application and rejection for fixed (DC) excited system with no controller. The 2nd order best fit curve represents the turbine power/speed characteristic, the 21 Ω and 28 Ω curves represent approximate values of the applied load resistance.

When a 1 kW step load was applied to the system with no ballast load frequency controller, the electrical power rises to around 3 kW with little variation in system speed. The trajectory then follows the new 21 Ω curve as the system slows to a new steady state operating point at about (44.5 Hz, 2250 W). A similar trajectory is shown for the load rejection transient.

Further investigation of the graphs in figure 3 reveals additional verification of the trajectories. The experiment to produce the parabolic graph involved starting the system with no ballast load connected, and maintaining a constant water head supplied to the turbine (in this case 16.4 metres). The unloaded system speed was around 1500 RPM resulting in a system frequency of approximately 50 Hz (and with greater water input, the unloaded turbine approached runaway speeds – 65 Hz^{+}). Ballast load resistors were then switched in manually, and the system speed and electrical power generated recorded. The graph shows four significant steps where the manual adjustment of the binary weighted resistive loads took some time to switch. The shape of the top sections of the trajectories immediately following the four main switching events (eg. from 30 Hz to 27 Hz) tracks the shape of the equivalent ballast resistance connected. Comparison with figure 10 suggests this trajectory is a result of the 6 Ω load.

In comparison, analysis of an AVR controlled excitation yields a significantly different set of resistive load power curves on the turbine curves. These are shown in figure 12, and again, the intersections of two curves represent a steady state operating point.

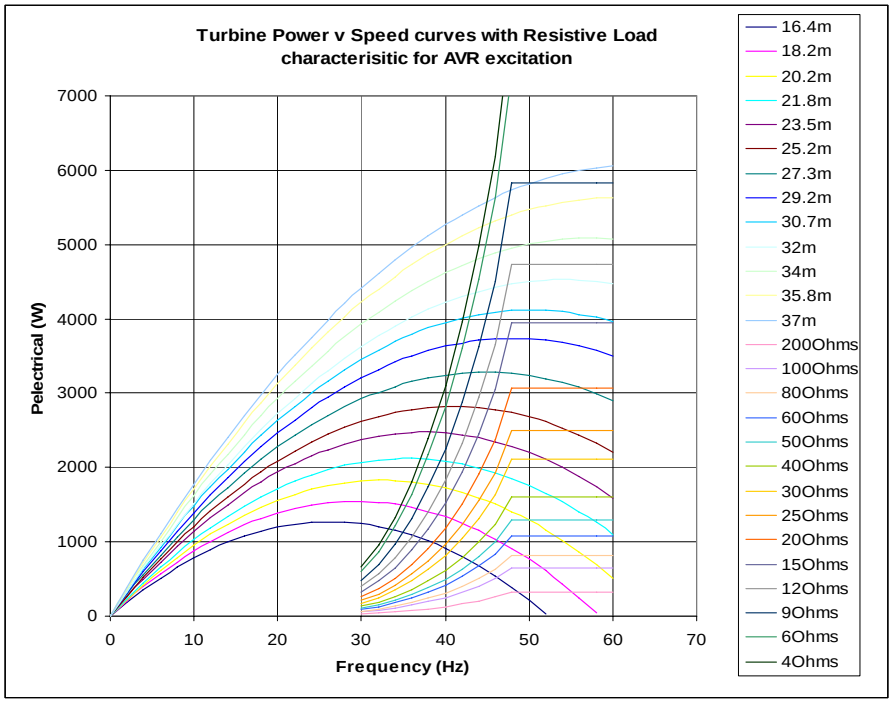

Figure 12. Steady state electrical power versus frequency for various water head input, with various Resistive Load characteristic curves for AVR controlled excitation.

The flat part of the resistive power curves results from AVR operation, it maintains constant terminal voltage, and hence constant power. The under frequency roll-off characteristic in this theoretical model was set at 47 Hz and excitation is reduced according to the graph shown in Figure 9. In practice, the UFRO can be adjusted, a typically (Australian) factory setting is around 45-46 Hz.

Figure 13 shows recorded data plotted as a trajectory overlaid on a parabolic turbine power speed curve (labelled 2nd order best fit) and theoretical resistive power curves for AVR with UFRO set at 46Hz. As before, the initial steady state operating point exists at (50 Hz, 2000 W). For the system with no ballast load frequency controller, when a 1 kW load is applied, the trajectory plots the path to the new steady state operating point at (44 Hz, 2300 W). Note that the system power remains approximately constant until the system speed reaches the UFRO set point. A similar trajectory is shown for the load rejection transient.

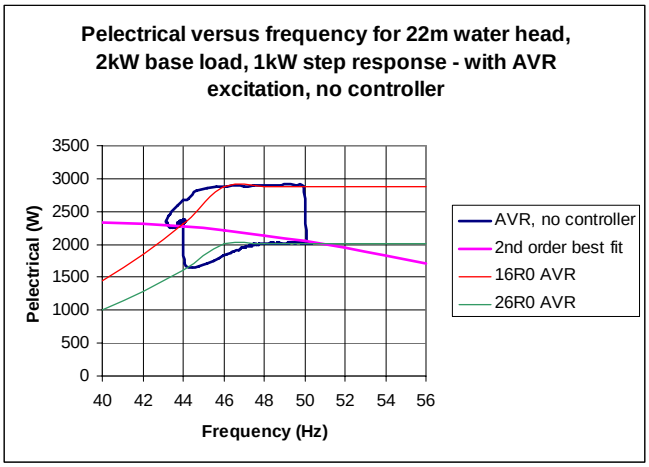

Figure 12 - Trajectory for P_{elect} during load application and rejection for AVR excited system with no controller.

8. Operating on the negative or positive side of the turbine power-speed curve.

Operating on the negative slope of the power speed curve will result in a trajectory towards new steady state operating point which opposes the change in demand, and will therefore assist speed regulation. However, the change in speed over this trajectory for an AVR excited system is faster than the fixed DC excited system.

Operating on the positive slope will result in a trajectory towards a new steady state operating point which, in the case of an increase in demand, cannot be sustained, and will therefore hinder speed regulation action. As a result, an AVR excited systems cannot be brought to a steady state condition; ie. it is not possible to bring the system up to a nominal speed as is the case with an externally governed system such as a diesel engine prime mover [6].

From observations of the system operating on either slope, it is evident that the AVR readily ‘drops into’ the UFRO condition, and tends to stay there in a reduced excitation stable operating condition. This aligns with observations of others [5]. Where installed, a ballast load controller will respond to this low frequency operating point by reducing ballast load. But the return trajectory out of the UFRO condition usually requires a significant change in ballast load, and as a result, the system speed increases rapidly, overshoots the nominal set-point, and the similar response rates of the load controller and AVR result in the system returning to UFRO condition. This is the oscillation shown in figure 8.

9 Conclusion

The observations of unsatisfactory performance and instability in micro-hydroelectric systems resulting from the interaction of the ballast load frequency controller and automatic voltage regulators have been verified. System modelling yields analysis suggesting the similar time constants of the two feedback systems (speed and voltage) contribute to instability.

The Under Frequency Roll-Off (UFRO) characteristic of AVR excited systems results in a reduced excitation steady state operating point. The system frequency at this steady state operating point is not necessarily the UFRO set-point, but is dependent on hydraulic power input.

This study also yields an understanding of the possible steady state operating points on the turbine power speed curves for constant excitation and for AVR controlled excited systems. Constant excitation permits operation on the positive or negative slope of the curve, whilst stable operation is only possible on the negative slope side of the curve for the AVR excited system.

Acknowledgements

We acknowledge the critical contribution to field work made by APACE volunteers and the continued support of the Faculty of Engineering at the University of Technology, Sydney in making further research and development work in this field possible.

* APACE VFEG is a non-profit development assistance agency, implementing micro hydroelectric schemes over the past 20 years. Further information about the APACE VFEG projects can be found at www.apace.uts.edu.au.

References

[1] Jarman R, Bryce P. Manawai Harbour micro hydroelectric scheme: a case study in appropriate technology transfer. International Small Islands Studies Association (ISISA) Conference, Isle of Skye, 16-20 October, 2000.

[2] Pio NS, Tutua J. Village power in Solomon Islands – a grassroots development. Energia News 2004; Vol.6 No.2, p. 14-6

[3] R. Waddell R, Bryce P. Micro-hydro systems for small communities. Renewable Energy 16, 1999, p.1257-61

[4] Chehu F, Kohler R. Control system for mini hydro plants. Water Power and Dam Construction, Jan.1989, p. 25-6.

[5] Fischer G, Arter A, Meier U, Chapallaz JM. Harnessing Water power on a Small Scale – Vol. 8 Governor Product Information. SKAT Swiss Centre for Appropriate Technology, St.Gallen, 1990, p. 8

[6] Newage International, SA465 Automatic Voltage Regulator (AVR) Specification, Installation and Adjustments. Newage International Limited, Stamford; 2000, p. 3

[7] Harvey A. Micro-hydro design manual – A guide to small-scale water power schemes. Intermediate Technology Publications, London, 1993; p. 266

[8] Fraenkel P, Paish O, Harvey A, Brown A, Edwards R, Bokalders V. Micro-hydro Power - A Guide for development workers. Intermediate Technology Publications, London, 1991; p.106

[9] Elsedawi IR, Elassal AH, Azzouz EM. Effects of AVR systems on the performance of Synchronous generators. CCECE'97 – IEEE, 1997; p. 47-50

[10] Portegijs J. The humming bird electronic load controller/induction generator controller. ENECO Dutch energy distribution company, humbird.zip downloaded from www.geocities.com/wim_klunne/hydro/egroup/portegijs.html on 17 June 2001; p. 128

[11] Hagen DL. Developments in controls to govern mini- and micro-hydropower systems. Renewable Energy Review Journal, Vol. 8, No. 2, December 1986; p. 86-101

[12] Robinson P, Kormilo S. Recent advances in the development of microcontroller based electronic load controllers, First International Conference on Small Hydro organized by International Water Power and Dam Construction, Hyatt Regency Hotel, Singapore,13-16 February, 1984

[13] Kormilo S, Robinson P. Electronic control of small hydroelectric schemes using a microcomputer. IEE Proceedings, Vol 131, Pt E, No. 4, July 1984; p. 132-6.

[14] Henderson D. Recent developments of an electronic load governor for micro hydroelectric generation. IEE Renewable Energy, Conference publication No. 385, 17-19 November 1993; p. 84-8

[15] Elder JM, Boys JT, Woodward JL. Integral cycle control of stand-alone generators. IEE Proceedings, Vol 132, Pt C, No. 2, March 1985; p. 57-66

[16] Hino Motors Ltd. Hino WO4D – Diesel Engine for Industrial use – Technical Data. Hino Motors Ltd Public relations Office, Tokyo, 2000.

[17] Thake J. The micro-hydro turbine manual: design, manufacture and installation for small scale hydropower. ITDG Publishing, London, 2000; p. 38

[18] Carlson AB, Gisser DG. Electrical Engineering – Concepts and Applications. Addison-Wesley, Reading, Massachusetts, 1981; p721-3

[19] IEEE Recommended Practice for Excitation Systems Models for Power Systems Stability Studies, IEEE Standard 421.5-1992, New York, 10 August 1992, p. 51

[20] Basler AVC63-2.5 AVR Instruction Manual datasheet, Rev A, March 1998 downloaded from www.basler.com 3 August 2005